Supporting Information for:

Nonequilibrium surfactant partitioning into microdroplets generates local phase inversion conditions and interfacial instability

Samuel G. Birrer[1], Sanjana Krishna Mani[1], Bryan Kaehr,[2] Ayusman Sen,[2,3,4,5] Lauren D. Zarzar[1,4,5]*

1. Department of Chemistry, The Pennsylvania State University, University Park, PA 16802, USA
2. Advanced Materials Laboratory, Sandia National Laboratories, Albuquerque, NM 87185, USA
3. Department of Chemical Engineering, The Pennsylvania State University, University Park, PA 16802, USA
4. Department of Materials Science and Engineering, The Pennsylvania State University, University Park, PA 16802, USA
5. Materials Research Institute, The Pennsylvania State University, University Park, PA 16802, USA
*Corresponding, ldz4@psu.edu

This supporting information document contains:

1. Supporting figures
2. Supporting tables
3. Descriptions of supporting videos
4. Supporting calculations

1. Supporting figures

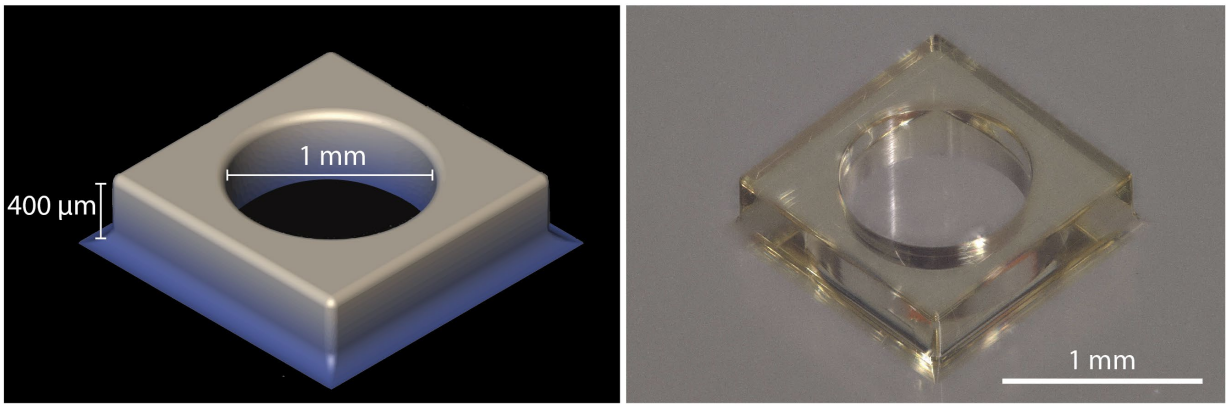

Figure S1. Schematic and photograph of the well used for droplet cluster containment. This structure was used for experiments investigating droplet number density effects, described in Figure 5.

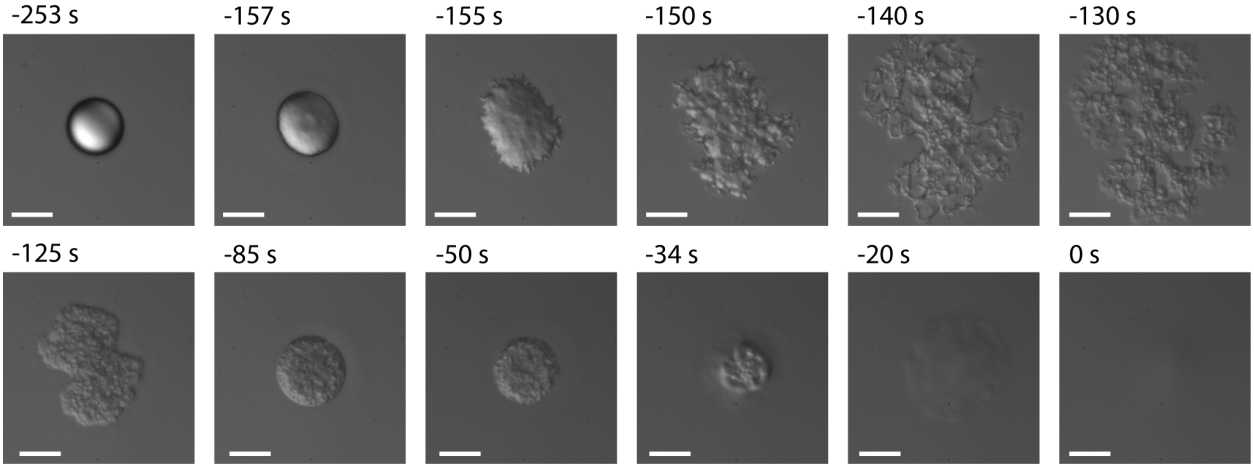

Figure S2. Time-series DIC micrographs of explosion of 1-bromobutane droplet in 0.1 wt% Tergitol NP-9. The protrusions and cavities formed during dissociation are visible from -155 s to -130 s, as well as the reformation of a spherical droplet shape from -125 s to -85 s, with aqueous-rich inclusions retained in the interior. Captured using Nikon Ti-U. Scale = 25 μm.

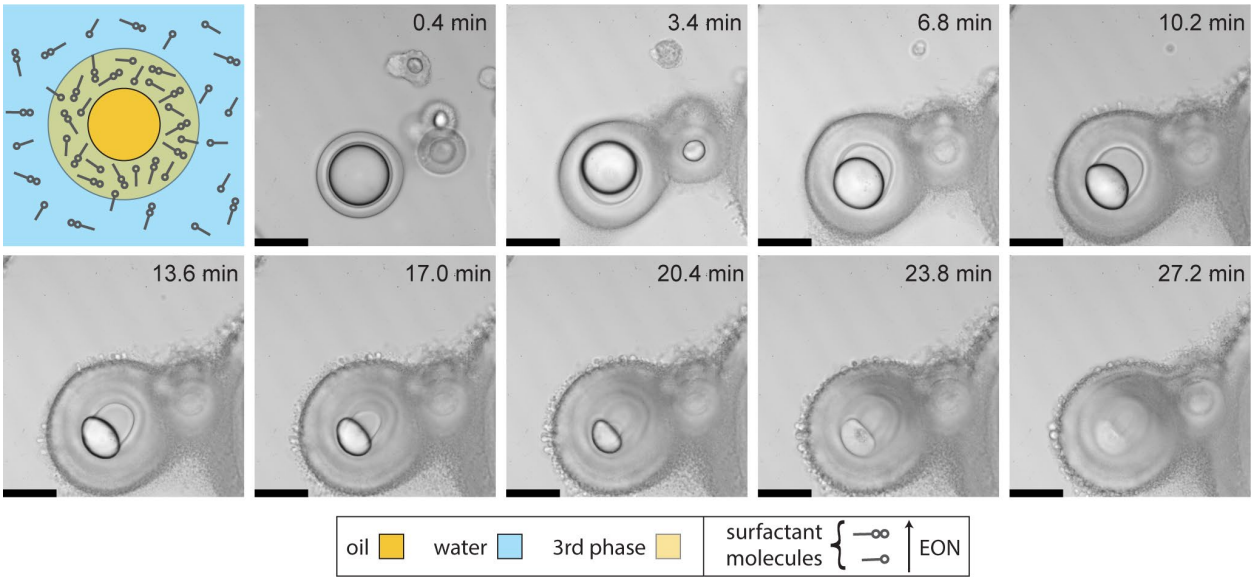

Figure S3. Droplets in high concentrations of low-EON surfactants form an additional phase between water and oil. General schematic, followed by time-series micrographs of several bromobutane droplets in 10 wt% Tergitol NP-9. See **Video S5** for full sequence. Scale = 100 μm.

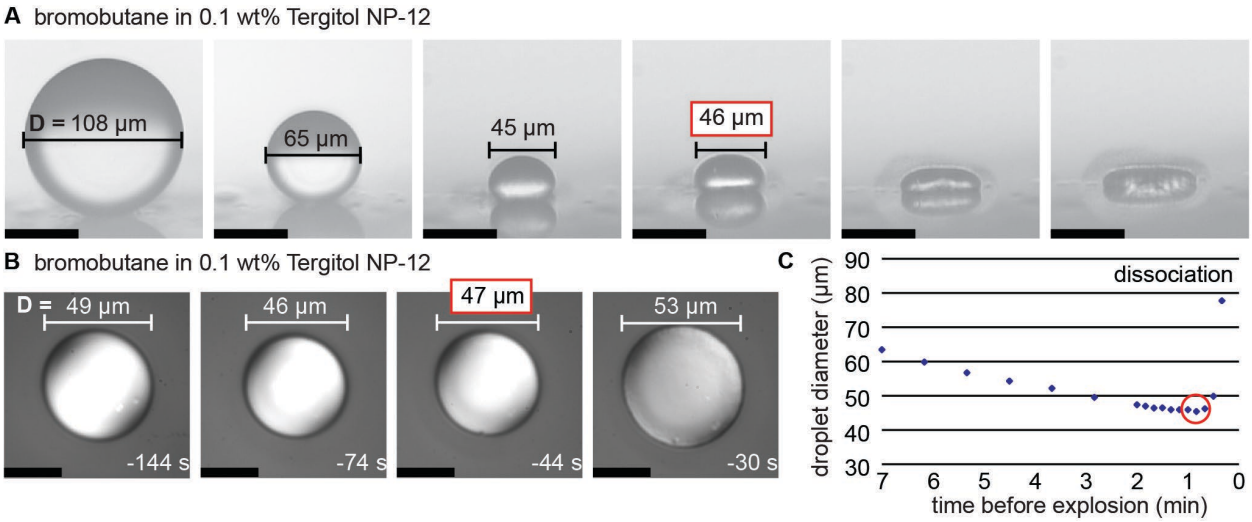

Figure S4. Method for assigning the diameter of droplets near the time of dissociation. (A) Side view micrograph series showing how droplets flatten and reach a point at which their horizontal diameter begins to grow larger due to droplet flattening. Scale = 50 µm. **(B)** DIC micrograph series showing the appearance of a droplet under the same oil and surfactant conditions as (A) but viewed in an inverted optical microscope. Scale = 25 µm. **(C)** Plot of droplet horizontal diameter from the same droplet in (B) as measured with ImageJ. Time 0 represents the first observation of interfacial protrusions as in the third frame in **Figure S1**), while the red circle indicates the point where the diameter began to grow, which is the diameter reported in **Figure 2B**.

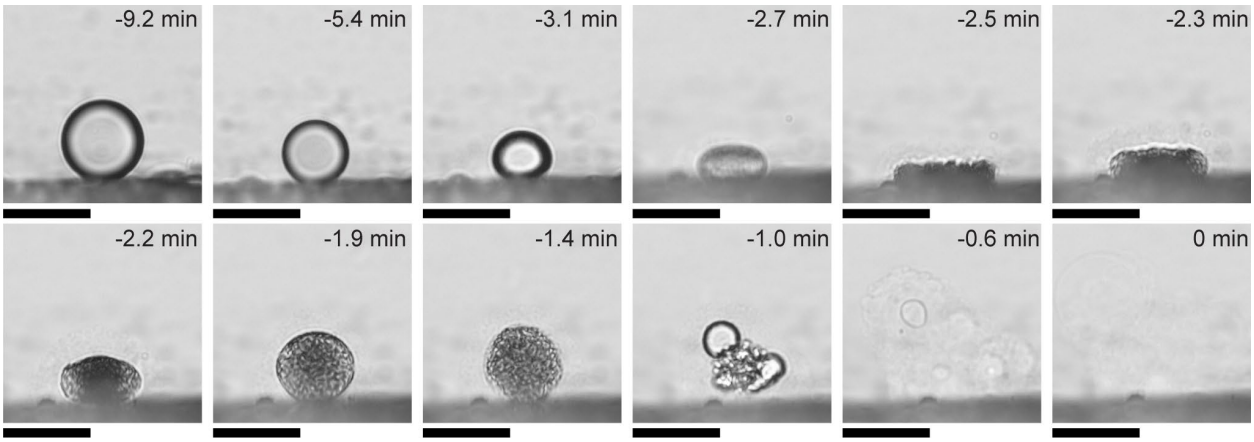

Figure S5. Surfactant partitioning and solubilization leads to droplet flattening, impacting how dissociation diameter is determined. Side-view, time-series micrographs of a bromobutane droplet in 0.1 wt% Tergitol NP-12 sitting on the bottom of a cuvette showing drop flattening and dissociating. Scale = 50 µm. After the phase inversion conditions dissipate, the remnants of the droplet return to a spheroidal shape, as seen in the -2.2 min, -1.9 min and -1.4 min timepoints. This is probably a coalescence of the oily phase around a large volume of newly formed aqueous inclusions, which subsequently merge with one another and with the continuous phase. Though we have not studied this portion of the behavior in detail, we hypothesize that this is due to a restoration of some interfacial tension and recoalescence of the leftover oil and surfactant when the special mixture of low-EON surfactant that precipitated the event has had some time to diffuse away. The newly formed droplet is clearly quite different in composition from the droplet before dissociation, because it subsequently dissolves by a gradual fading of the visible interface (in the -0.6 min and 0 min timepoints), suggesting a high concentration of surfactant and water relative to oil.

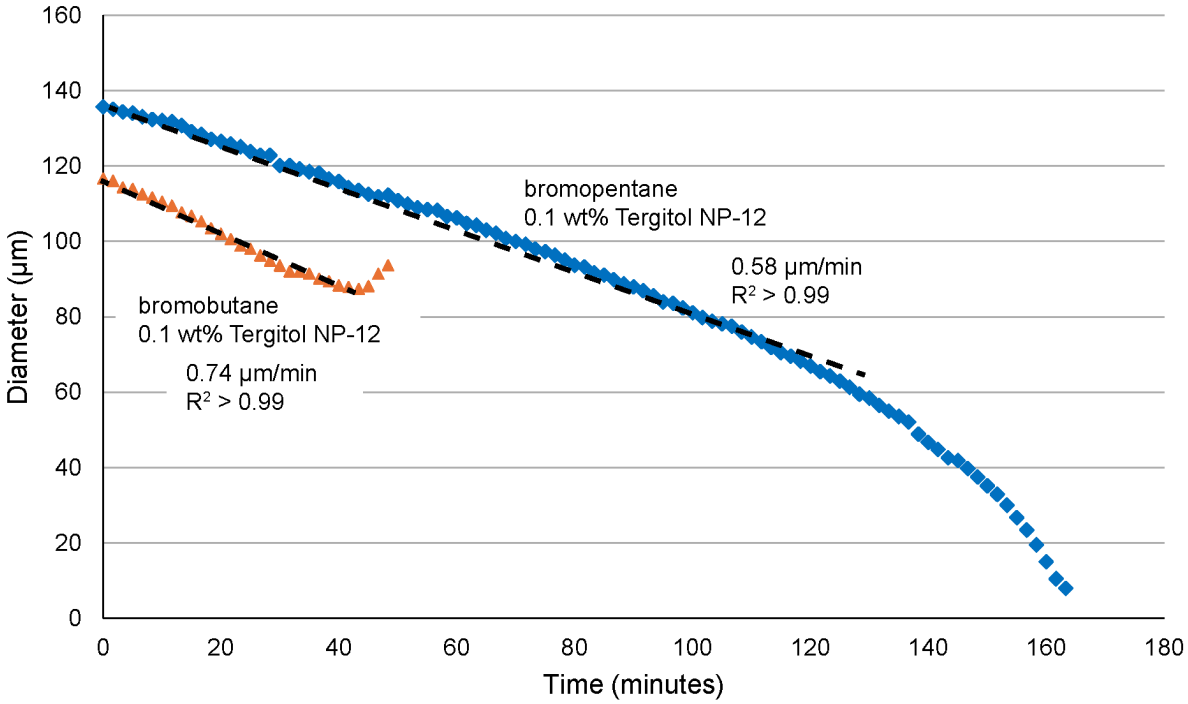

Figure S6. Plot of diameter over time for a droplet of bromobutane and a droplet of bromopentane in 0.1 wt% Tergitol NP-12. The bromobutane droplet dissociates, showing an apparent fishhook shape at the end due to flattening, since this data is collected by observing the diameter by inverted microscope. The bromopentane droplet does not dissociate, and solubilization rate increases near the end due to the increased surface area-to-volume ratio. The square of the radius would show a linear relationship here. For both, the solubilization rate in µm/min is calculated using a mostly linear portion of the data.

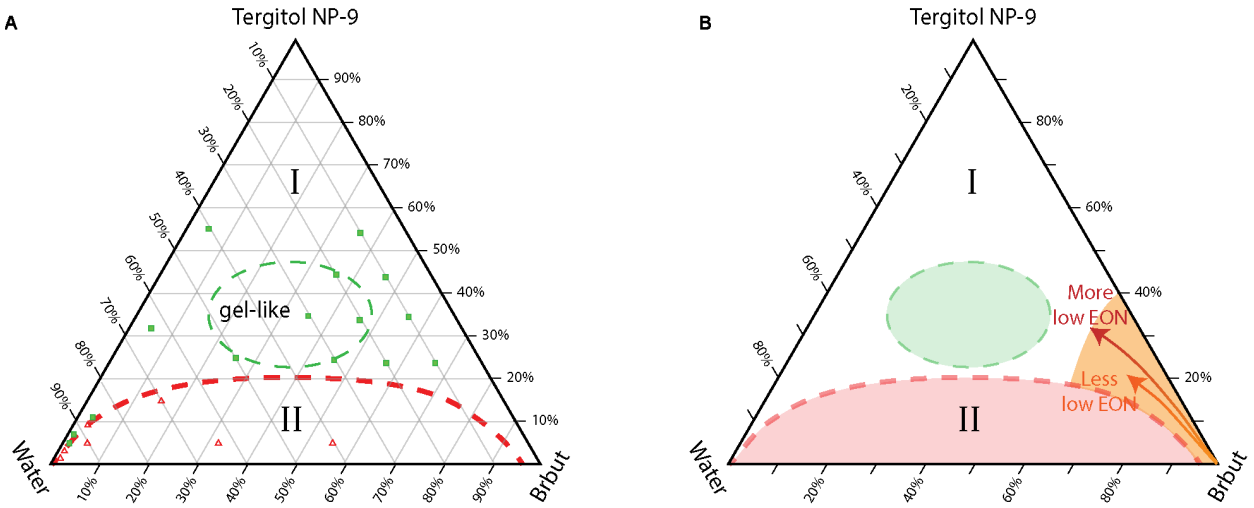

Figure S7. Pair of pseudo-ternary phase diagrams depicting a rough idea of what may occur as the droplet composition develops over time. The boundaries of the two-phase and gel-like regions are extremely approximate, as they will vary depending on the distribution of the EON, which we know is changing over time in the local vicinity of the droplet. The green and red points on the lefthand diagram in **A** show some compositions that were tested in bulk to roughly confirm 1-phase or 2-phase type behavior. The arrows in the righthand diagram in **B** show how we anticipate that a droplet with access to more low-EON surfactant will proceed farther into the interior of the phase diagram before reaching a steady state concentration of surfactant, as it will be able to uptake more surfactant.

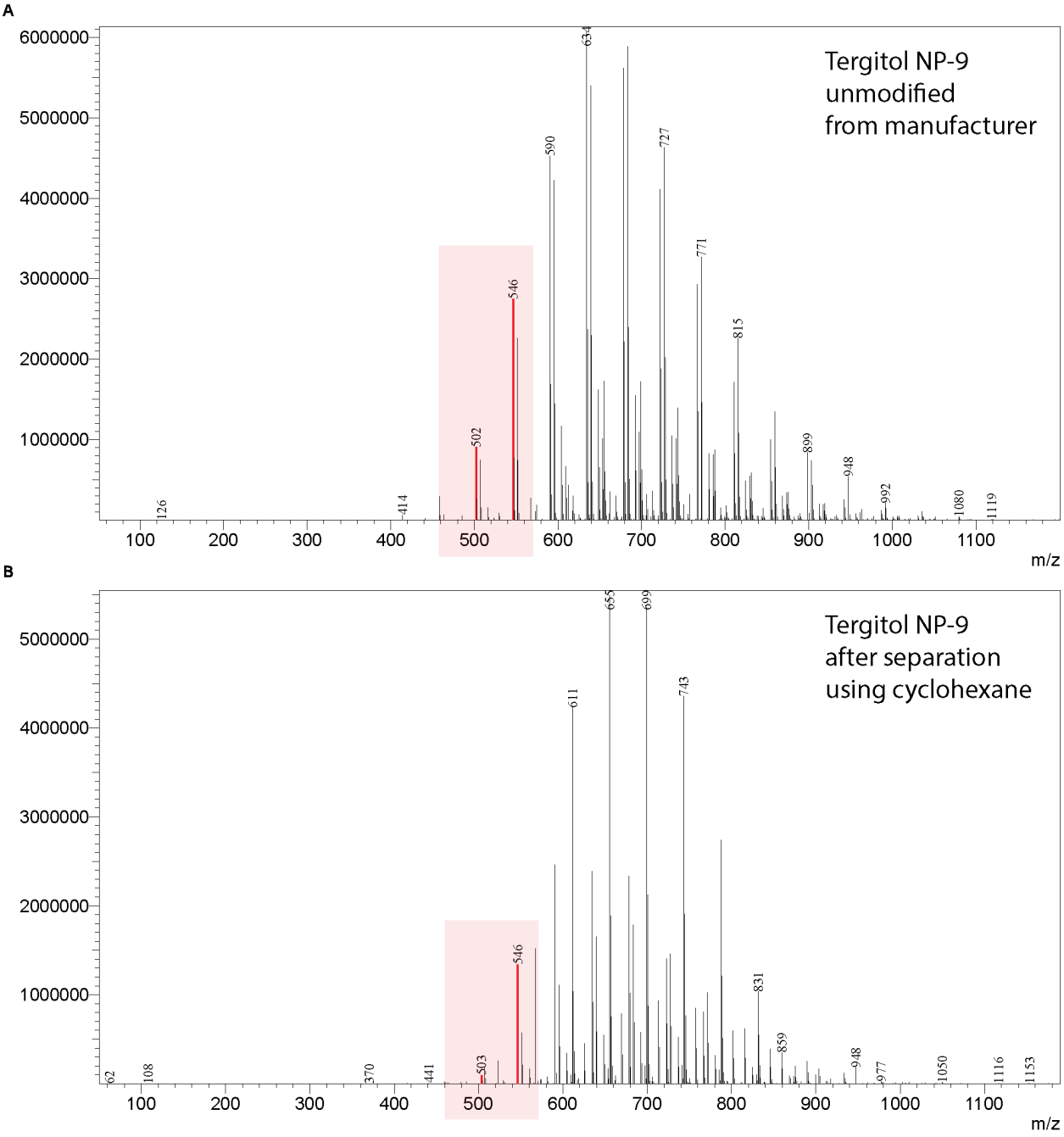

Figure S8. Mass spectrograms showing the change in the distribution of Tergitol NP-9 after a simple separation using cyclohexane and water, removing some of the lowest EON fractions. (A) Tergitol NP-9 as provided by the manufacturer. **(B)** Modified Tergitol NP-9 after cyclohexane and water separation, showing reduced peaks at the lower EON values (highlighted with red box) indicative of smaller quantities of low-EON surfactant present.

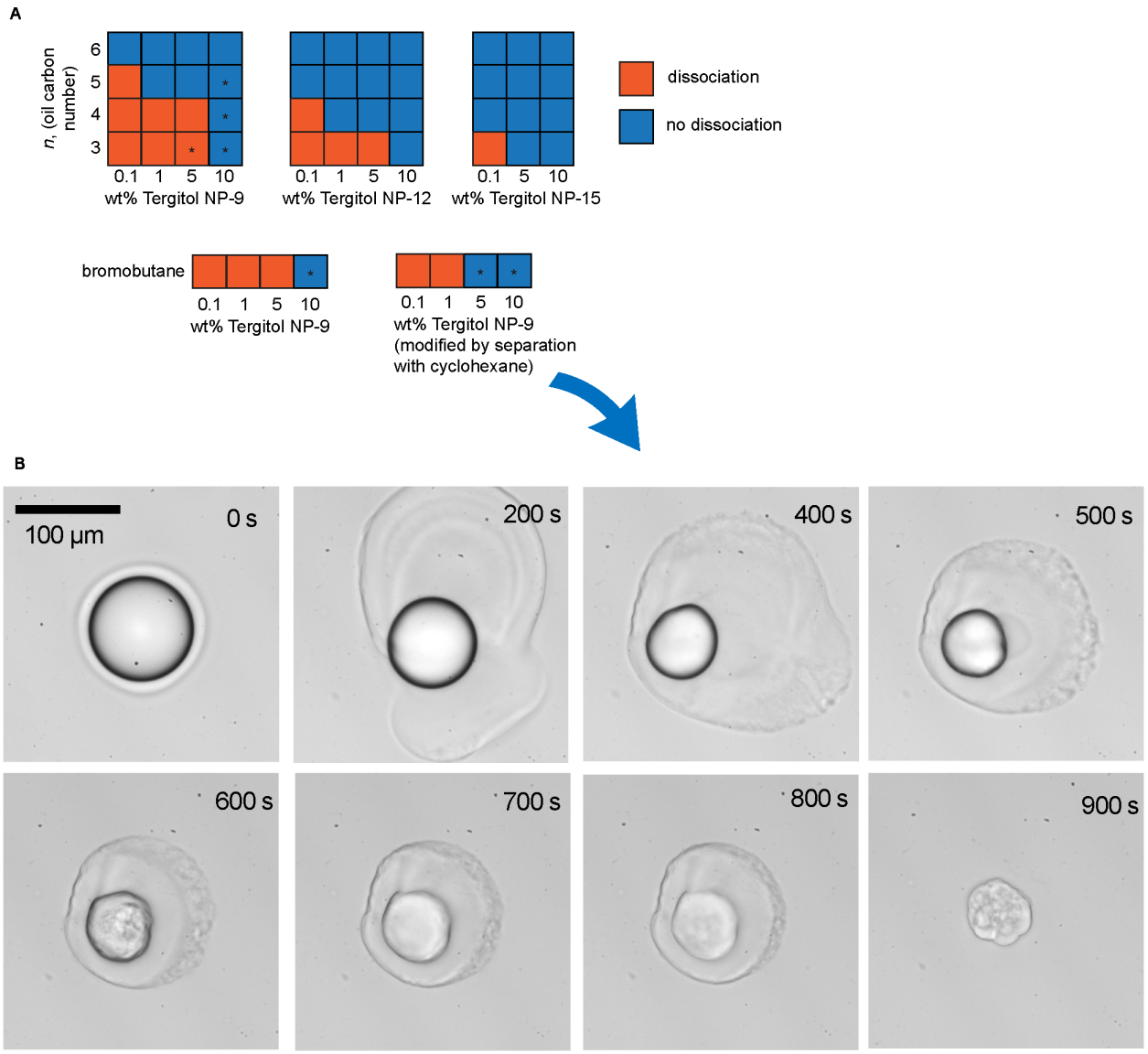

Figure S9. Revisited grid plot and image sequence showing the non-dissociating behavior of a bromobutane droplet in a 5 wt% solution of Tergitol NP-9 *after* depletion of lowest-EON fraction. The separation was carried out in a separatory funnel using 50 mL of deionized water containing 3 mL of Tergitol NP-9 and 50 mL of cyclohexane. While rapid solubilization still occurs, there is no recognizable dissociation such as we observed in the same concentration of unmodified Tergitol NP-9, and the oil-water interface gradually fades away instead.

2. Supporting Tables

Table S1. Linear fit R-squared values for the data in Figure 2b.

Oil / surfactant / concentration	B (ii,iii)	B (i,ii)
	Coefficient of Determination (R-squared)	
Bromobutane / Tergitol NP-9 / 0.1 wt%	0.90	0.91
Bromobutane / Tergitol NP-9 / 1.0 wt%	0.73	0.66
Bromobutane / Tergitol NP-12 / 0.1 wt%	0.79	0.79
Bromopentane / Tergitol NP-9 / 0.1 wt%	0.98	0.91
Bromopropane / Tergitol NP-9 / 0.1 wt%	0.92	0.99

3. Supporting video descriptions

Video S1. A DIC microscopy video showing prototypical solubilization behavior of *n*-bromobutane in 1 wt% Tergitol NP-12, captured using a Nikon Ti-U inverted microscope.
Video S2. A fluorescence microscopy video showing a droplet of *n*-bromobutane solubilizing in 1 wt% Tergitol NP-12 with Nile Red, captured using a Zeiss Axio Observer inverted microscope with Zeiss Filter Set 91 HE LED. Nile Red is a dye that solubilizes easily, so it does not build up significantly inside the droplet during the experiment.
Video S3. A fluorescence microscopy video showing a droplet of bromobutane solubilizing and dissociating in 0.1 wt% Tergitol NP-12 with Nile Red, captured using a Zeiss Axio Observer inverted microscope with Zeiss Filter Set 91 HE LED.
Video S4. A DIC microscopy video showing a droplet of bromobutane solubilizing and dissociating in 0.1 wt% Tergitol NP-12, captured using a Nikon Ti-U inverted microscope.
Video S5. Brightfield microscopy video showing the formation of a distinct third phase surrounding droplets of bromobutane in 10 wt% Tergitol NP-9, captured using a Nikon Ti-U inverted microscope.

4. Supporting Calculations

To establish an upper bound to the interfacial tension when droplets began to become deformed from a spherical shape, we used the Bond number (or Eötvös number), which relates the gravitational forces promoting such deformation to the interfacial tension counteracting it, and takes the form:

$$Bo = \frac{\Delta\rho g L^2}{\gamma_{ow}} \quad \text{(S1)}$$

where $\Delta\rho$ is the density difference between the phases, g is the gravitational constant, L is the radius of curvature of the droplet, and γ_{ow} is the interfacial tension. When Bo > 0, gravitational deformation impacts the droplet shape, and the larger the difference in density between the phases, the greater the gravitational force. So, if we make a conservative estimate of ρ_o, the density of the oil phase, we can place an upper bound on the interfacial tension at the point where the droplet begins to deform. The conservative estimate of the droplet density is taken to be ρ_o = 1.27 g/mL, which is the density of the pure bromobutane oil and assumes that the partitioning of surfactant does not change the droplet density at all.

Using this conservative estimate on the droplet in **Figure S5**, we can estimate γ_{ow} to be 5.95 x 10^{-4} mN/m. If, alternatively, we assume that the new density of the droplet after extensive partitioning is roughly the same as that of pure Tergitol surfactant, 1.05 g/mL, then the estimated γ_{ow} is 1.10 x 10^{-4} mN/m. If we assume that the contributions of each liquid to the density are perfectly proportional to their fraction in the mixture, and that the mixture is approximately 1:4 surfactant to oil, then ρ_o = 1.23 g/mL, and γ_{ow} = 5.07 x 10^{-4} mN/m.

The same calculations for the larger droplet (radius = 32 μm) in **Figure S4A** give values of 5.02 x 10^{-4} mN/m, 2.31 x 10^{-3} mN/m, and 2.71 x 10^{-3} mN/m for the same lower limit, best estimate, and upper limit. So, although it is still imperfect due to assumptions that may not hold, our calculations give a reasonable order of magnitude estimate of 1 x 10^{-4} mN/m to 3 x 10^{-3} mN/m based on our two extreme assumptions of the droplet density.